

## Mass Transport Velocity in Shallow-Water Waves Reflected in a Rotating Ocean with a Coastal Boundary

FRODE HOYDALSVIK\*

*Mohn-Sverdrup Center, Nansen Environmental and Remote Sensing Center, Bergen, Norway*

(Manuscript received 21 January 2006, in final form 5 February 2007)

### ABSTRACT

The mass transport velocity in shallow-water waves reflected at right angles from an infinite and straight coast is studied theoretically in a Lagrangian reference frame. The waves are weakly nonlinear and monochromatic, and propagate in a homogenous, viscous, and rotating ocean. Unlike the traditional approach where the domain is divided into thin boundary layers and a core region, the uniform solution is obtained here without constraints on the thickness of the bottom wave boundary layer. It is shown that the mass transport velocity is not only sensitive to topography, but depends heavily on the interplay between the vertical length scales. Similarities and differences between the cases of a constant depth, a linearly sloping bottom, and a wavy and linearly sloping bottom are discussed. The mass transport velocity can be divided into two main categories—that induced by waves with a frequency close to the inertial frequency, and that induced by waves with a much larger frequency. For waves significantly affected by rotation to first order, the cross-shore mass transport velocity is very small relative to the alongshore mass transport velocity, and the direction of the mass transport velocity is reversed relative to that in waves of much higher frequencies.

### 1. Introduction

The investigation of the mass transport velocity in reflected water waves has a long history (e.g., Rayleigh 1883; Longuet-Higgins 1953; Ünlüata and Mei 1970; Dore 1970; Liu and Davies 1977; Lamoure and Mei 1977; Craik 1982). The existence of mean recirculation cells as those originally found by Rayleigh (1883) and Longuet-Higgins (1953) has been confirmed both experimentally and theoretically, and it has been shown that reflection from a vertical boundary has importance for the formation of half-wavelength sandbars on the sea bottom (Herbich et al. 1965; Carter et al. 1973; Yu and Mei 2000).

The physical mechanism of the recirculation cells in a nonrotating frame is well known (e.g., Rayleigh 1883; Longuet-Higgins 1953; Mei 1983). However, the details of the vertically varying mean particle velocity in a rotating frame is yet not fully clear. Traditionally, the

theoretical investigation of the mean mass transport in long ocean waves affected by rotation and topography has been focused on the vertically integrated transport in tides (e.g., Huthnance 1973, 1981; Zimmerman 1978, 1979; Loder 1980).

Common, simplifying assumptions applied in the analytic study of the mass transport velocity in ocean waves are the assumptions of a constant depth and a thin wave boundary layer. Hunt and Johns (1963) discussed the vertically varying mass transport velocity profile in tides and long waves, but only for the top of a thin bottom wave boundary layer, and for a constant depth. While retaining the assumptions of a constant depth and a thin wave boundary layer, Lamoure and Mei (1977) extended the theory of Hunt and Johns (1963), and discussed the tidally induced near-bottom mass transport in the vicinity of small two-dimensional bodies.

Wright and Loder (1985) studied (weakly nonlinear) topographic rectification of tidal currents, under the assumption of no along-isobath variation. Similar to Huthnance (1973) and Loder (1980), Wright and Loder found anticyclonic mean circulation around shallow regions in the case of weak friction. However, they did not consider the mean flow in the wave boundary layer, and they applied the rigid-lid approximation. This approximation makes their theory inapplicable for shal-

---

\* Current affiliation: The Norwegian Meteorological Institute, Oslo, Norway.

---

*Corresponding author address:* Frode Hoydalsvik, Mohn-Sverdrup Center, Nansen Environmental and Remote Sensing Center, Thormøhlensgt. 47, N-5006 Bergen, Norway.  
E-mail: frode.hoydalsvik@nersc.no

low-water waves of a higher frequency, where oscillations of the free surface are important. It has also been shown that the effect of free-surface oscillations on the residual current of the semidiurnal tide can be important (e.g., Tee 1985). Dong et al. (2004) extended the theory of Wright and Loder to study the residual recirculation in tidal fronts over a sloping bottom, taking into account a prescribed density field. Although they accounted for a free surface, they applied the dynamic (free shear) boundary condition at a fixed horizontal level. If the rigid-lid assumption is not used, their theory requires implicitly the wave boundary layer and bottom Ekman layer to be thin in comparison with the depth.

For low-frequency waves such as tidal waves, the assumption of a thin wave boundary layer often does not hold in shallow shelf seas (e.g., Soulsby 1983). Ianniello (1979) recognized this. However, he studied the tidally induced residual currents in narrow inlets where the Kelvin number was small enough for the effect of rotation on the primary wave field to be negligible.

In this paper, I seek to illustrate in what way the mass transport velocity in Poincaré waves may react to the Coriolis force as compared with the mass transport velocity in enduring waves of a much higher frequency. Unlike the latter waves, the former are significantly affected by the earth's rotation to first order. The focus is then different from that of recent papers on wave-current interaction wherein the effects of topography and Coriolis force are discussed (e.g., Restrepo 2001; McWilliams et al. 2004). I aim to study the joint effect of the Coriolis force, wave damping, friction, and reflection, without constraints on the wave boundary layer thickness. This model is meant to complement earlier studies, some of which may focus on important effects not considered here: multiple fluid layers (e.g., Dore 1970; Ng 2004), two-dimensional wave propagation (e.g., Hunt and Johns 1963; Lamoure and Mei 1977; Iskarandi and Liu 1991), propagation of water wave packets (e.g., Grimshaw 1981), feedback from a slowly evolving bottom profile (e.g., Yu and Mei 2000; Restrepo 2001), interaction with currents and/or topography (e.g., McWilliams and Restrepo 1999; Restrepo 2001; McWilliams et al. 2004), and transport and resuspension of fine particles (e.g., Mei et al. 1998).

The present paper is organized as follows: In section 2 the problem is formulated mathematically using regular perturbations in Lagrangian coordinates. In section 3, time-periodic, complex Fourier components for the primary wave field are considered, and a set of equations for the first-order solution is derived. From the solution that is found here, the governing equations for the mass transport velocity to second order, valid for a wave boundary layer of general thickness and a two-

dimensional, rotating ocean, are derived and solved in section 4. The solution is discussed for the aforementioned cases of bottom configuration, in section 5, for waves with a period of 5 min and, in section 6, for waves at the semidiurnal tidal frequency. A summary and some concluding remarks are given in section 7.

## 2. Mathematical formulation

I consider shallow-water waves that propagate toward the shore at normal incidence. They are forced, monochromatic, and barotropic. It is assumed that the water is well mixed, with negligible density variation. The effect of wind stress, varying surface pressure, and currents not forced by the wave field will be omitted from this discussion. The alongshore variation is neglected, that is, the coast and isobaths are assumed to be both straight and parallel.

The motion is described in a Cartesian coordinate system with its origin on the seafloor. The  $z$  axis points up the vertical, the  $y$  axis is directed along an isobath, and the  $x$  axis points perpendicularly toward the coast (Fig. 1). In the equilibrium state without the presence of waves,  $z = H_0$  at the surface. When the wave field is established, the surface is described by  $z = H_0 + \zeta_0(x, y, t)$ . Let a fluid particle be described by its Lagrangian label coordinates  $(a, b, c)$ . Its position  $(x, y, z)$  at time  $t$  will be a function of  $t$  and  $(a, b, c)$ . The velocity and acceleration of the particle are  $(x, y, z)_t$  and  $(x, y, z)_{tt}$ , respectively.

Given the idealized model setting, it suffices to parameterize turbulent friction with a constant eddy viscosity  $\nu_0$ , neglecting lateral friction (e.g., Mei et al. 1998). In fact, Davies et al. (2001) found that a constant eddy viscosity could reproduce elevations and currents in tidal waves as accurately as those based on a Prandtl model. However, it is difficult to find a realistic, representative value for the constant eddy viscosity. An eddy viscosity is chosen with values within typical ranges reported earlier in literature,  $\nu_0 \sim 10^{-5}$ – $10^{-1} \text{ m}^2 \text{ s}^{-1}$ , where the lower bound is more representative for the interior of the ocean and the upper bound is more typical for shallow areas with strong tidal mixing; see, for example, Pond and Pickard (1983). Mei et al. (1998, see also references therein) suggest that  $\nu_0 \sim 2 \times 10^{-2} \text{ m}^2 \text{ s}^{-1}$  for a smooth mud bed and  $\nu_0 \sim 5 \times 10^{-2} \text{ m}^2 \text{ s}^{-1}$  for a rippled sandy bed. It is assumed that if one studies shallow-water waves in the vicinity of a coast or shore, it is reasonable to pick values from the mid- or upper range of viscosity values.

By utilizing the fact that all variables (except of  $y$ ) are independent of  $b$ , the governing equations and boundary conditions at the bottom and the surface can be written as (see, e.g., Hoydalsvik and Weber 2003),

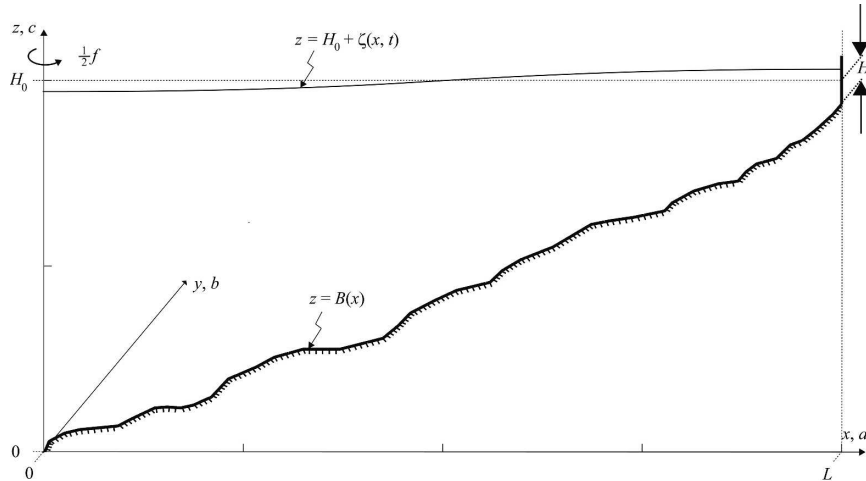


FIG. 1. Sketch of the system. Monochromatic shallow-water waves propagate from deeper waters toward the coast with normal incidence. At  $x = 0$ , the equilibrium depth  $D$  is  $H_0$ , and at the shore it is  $H_1$ . The (hypothetical) area of study ( $0 < x < L$ ) is chosen differently through the discussion, from the continental shelf ( $L$  is chosen to be large, of order 100 km) to the coastal or nearshore region ( $L \sim 1\text{--}10$  km). In all cases, a finite depth is chosen at the shore, and perfect reflection is assumed here. The wave amplitude to leading order at the shore is assumed to be known. The vertical scale is greatly exaggerated. The system is located on the Northern Hemisphere; i.e., the Coriolis parameter  $f$  is nonnegative.

$$W_t + ifW = -gJ(\zeta, z) + \nu_0 J[x, J(x, W)], \quad (2.1)$$

$$J(x, z) = 1, \quad (2.2)$$

$$W = 0, \quad z = B(x), \quad \text{and} \quad (2.3)$$

$$J(x, W) = 0, \quad z = \zeta + H_0. \quad (2.4)$$

Here,  $g$  is acceleration resulting from gravity,  $W = x_t + iy_t$  is the Lagrangian complex horizontal particle velocity, and  $J(M, N) = M_a N_c - M_c N_a$  is the Jacobian determinant;  $B$  is the Eulerian coordinate of the bottom profile with  $B(0) = 0$ . Equations (2.1) and (2.2) express conservation of momentum and mass, respectively.

The boundary condition (2.4) is derived by requiring the viscous tangential stresses  $[\tau^{(x)}, \tau^{(y)}]$  to vanish at the free surface (e.g., Davies 1985; Weber 1998; Ng 2004). It rests on the shallow-water assumption  $kD \ll 1$ , and is

valid to  $O(kD)$ , where  $k$  is the wavenumber and  $D = H_0 - B$  is the equilibrium depth. The assumption of a hydrostatic pressure in Eulerian coordinates in Eq. (2.4) requires  $kD \ll 1$  and a large Ursell number, for example,  $U = \zeta_0 k^{-2} D^{-3} \gg 1$ , where  $\zeta_0$  is the amplitude of the surface displacement (see the appendix) to leading order. Unless the latter requirement is fulfilled, there is little point in regarding nonlinear effects while disregarding nonhydrostatic effects; see, for instance, Blondeaux et al. (2002).

Apart from the shallow-water approximation and the idealized parameterization of turbulent friction, (2.1)–(2.4) are exact. I will attempt to find an approximate solution to the time-averaged mass transport velocity by following Pierson (1962). The small parameter  $\varepsilon = \zeta_0/H_0$  is defined, and I write

$$\left. \begin{aligned} \langle x, y, z \rangle &= \langle a, b, c \rangle + \varepsilon \langle x^{(1)}, y^{(1)}, z^{(1)} \rangle + \varepsilon^2 \langle x^{(2)}, y^{(2)}, z^{(2)} \rangle + \dots \\ \zeta &= \varepsilon \zeta^{(1)} + \varepsilon^2 \zeta^{(2)} + \dots \\ W &= \varepsilon W^{(1)} + \varepsilon^2 W^{(2)} + \dots \end{aligned} \right\}, \quad (2.5)$$

where the angle brackets denote vectors. Here, (2.5) is inserted into (2.1)–(2.4). From (2.5) one has  $c = H_0$ ,  $z^{(1)} = \zeta^{(1)}$ ,  $z^{(2)} = \zeta^{(2)}$ , and so on, at the surface. The slope given by  $z = B(x)$  in Eulerian coordinates corresponds to  $c = B(a)$  in Lagrangian coordinates.

This can readily be shown by utilizing (2.5) on the identity  $z = B(x)$ , and collecting terms with equal powers of  $\varepsilon$ . In case of a no-slip bottom condition, this is trivial, because the displacement at the bottom must be zero.

### 3. Analysis of the primary wave field

#### a. Solution by separation of variables

I write the surface displacement of the primary wave field on the following form:

$$\zeta^{(1)} = C(a)e^{i\omega t} + C^*(a)e^{-i\omega t} \quad (3.1)$$

(asterisk denotes complex conjugate). By utilizing this surface component, one gets the following system of equations to  $O(\varepsilon)$ :

$$W_t^{(1)} - \nu_0 W_{cc}^{(1)} + ifW^{(1)} = -g[C'(a)e^{i\omega t} + C'^*(a)e^{-i\omega t}], \quad (3.2)$$

$$x_a^{(1)} + z_c^{(1)} = 0, \quad (3.3)$$

$$\begin{aligned} W^{(1)} &= 0, & c &= B(a), \\ W_c^{(1)} &= 0, & \text{and } c &= H_0. \end{aligned} \quad (3.4)$$

Equation (3.2) suggests that one may split the solution for the horizontal velocity and displacement into two parts,

$$\begin{aligned} [W^{(1)}, x^{(1)}, y^{(1)}] &= (W_1, x_1, y_1)C'e^{i\omega t} \\ &+ (W_2, x_2, y_2)C'^*e^{-i\omega t}. \end{aligned} \quad (3.5)$$

Here, the functions with subscripts generally depend on  $a$  and  $c$ . By integrating the velocity in time, it is found that the components of the horizontal displacement can be written as

$$\begin{aligned} x_1 &= \frac{1}{2i\omega} (W_1 + W_2^*), & x_2 &= x_1^*, \\ y_1 &= -\frac{1}{2\omega} (W_1 - W_2^*), & \text{and } y_2 &= y_1^*. \end{aligned} \quad (3.6)$$

Associated with the components of the solution, a range of characteristic parameters are defined, such as frequencies  $\omega_1 = \omega + f$  and  $\omega_2 = \omega - f$ , bottom boundary layer thicknesses  $\delta_1 = (2\nu_0/\omega_1)^{1/2}$  and  $\delta_2 = (2\nu_0/\omega_2)^{1/2}$ , and complex vertical wavenumbers  $m_1 = (1 + i)/\delta_1$  and  $m_2 = (1 - i)/\delta_2$ . By inserting the form of  $W^{(1)}$  given by (3.5) into (3.2) and (3.4), one finds the components  $W_1$  and  $W_2$ ,

$$W_j = \frac{ig}{\omega_j} \left\{ 1 - \frac{\cosh[m_j(c - H_0)]}{\cosh(m_j D)} \right\}, \quad \text{for } j = 1, 2. \quad (3.7)$$

#### b. The eigenfunction for the surface elevation

By integrating the incompressibility equation to first order (3.3) over a water column, and using the fact that  $z^{(1)} = \zeta^{(1)}$  at the surface, one obtains

$$\zeta^{(1)} = - \int_B^{H_0} x_a^{(1)} dc = - \frac{\partial}{\partial a} \int_B^{H_0} x^{(1)} dc + x^{(1)} B_{a|c=B}, \quad (3.8)$$

where the rightmost term disappears resulting from the no-slip bottom boundary condition. By utilizing (3.1) and (3.5)–(3.8), it is found after some algebra that the eigenfunction  $C$  must satisfy

$$\frac{d}{da} \left[ D \left( 1 - \frac{\omega_2}{2\omega} \xi_1 - \frac{\omega_1}{2\omega} \xi_2^* \right) \frac{dC}{da} \right] + k_0^2 H_0 C = 0. \quad (3.9)$$

Here,  $\xi_j = \tanh(m_j D)/m_j D$  and  $k_0$  is the wavenumber for inviscid Poincaré waves over horizontal bottom,  $k_0 = (\omega^2 - f^2)^{1/2} (gH_0)^{-1/2}$ . By taking the leading-order surface amplitude to be  $\zeta_0$  and requiring perfect reflection at  $a = L$ , the boundary conditions for  $C$  become

$$C(L) = 0.5H_0 \quad \text{and} \quad C'(L) = 0. \quad (3.10)$$

When the depth is constant,  $D \equiv H_0$ ,  $C$  is readily found to be a damped trigonometric function,  $C = 0.5H_0 \cos(K\hat{a})$ , where  $\hat{a} = a - L$  and  $K = i\alpha + k = k_0 [1 - \omega_2 \xi_1 / (2\omega) - \omega_1 \xi_2^* / (2\omega)]^{-1/2}$ . Here,  $\alpha$  and  $k$  are the damping factor and the wavenumber, respectively, both of which are positive.

Consider the more physically realistic case of a bottom that slopes linearly upward from  $a = 0$ , where the depth is  $D = H_0$ , to the shore, where  $a = L$  and  $D = H_1$ . The bottom slope is  $\gamma = (H_0 - H_1)/L$ . The amplitude must be small relative to the depth, that is,  $\zeta_0 \ll H_1$ , otherwise the assumption of weak nonlinearities may not hold. In the discussion of Lentz et al. (2001), the slope on the midcontinental shelf is found to be around  $1.3 \times 10^{-4}$ , while the mean slope from the coast and 5 km away can be estimated as  $4 \times 10^{-3}$  (roughly 30 times as large). In such cases, the change of depth close to the coast is very abrupt for long waves, such as the semidiurnal tidal component (with typical horizontal lengths of  $\sim 10^6$  m). If one concentrates on the midcontinental shelf, it seems reasonable to take the near-coast region as a vertical wall, while considering the more moderate slope on the midcontinental shelf itself (e.g., Das and Middleton 1997).

When ignoring the effect of wave attenuation,  $C$  may be written as

$$C = \frac{G(a)}{G(L)} \left. \vphantom{C} \right\} \quad (3.11)$$

$$G(a) = \frac{1}{2} Y_0' \left( 2 \sqrt{\frac{\mu H_1}{\gamma}} \right) J_0 \left[ 2 \sqrt{\mu \left( \frac{H_0}{\gamma} - a \right)} \right] - \frac{1}{2} J_0' \left( 2 \sqrt{\frac{\mu H_1}{\gamma}} \right) Y_0 \left[ 2 \sqrt{\mu \left( \frac{H_0}{\gamma} - a \right)} \right]$$

where  $\mu = (\omega^2 - f^2)g^{-1}\gamma^{-1}$ ; see Das and Middleton (1997) who use a similar expression. In (3.11),  $J_0$  and  $Y_0$  are the first-order Bessel functions of first and second kind, respectively. Typical values for  $\gamma$  and  $\mu$ , when considering tidal waves on the continental shelf, are  $\gamma \sim 10^{-3}$  (typical slope of the shelf) and  $\mu \sim 10^{-6} \text{ m}^{-1}$  (assuming  $\omega \sim 10^{-4} \text{ s}^{-1}$ ); see, for instance, Battisti and Clarke (1982) and Das and Middleton (1997).

For the effect of wave attenuation on wave propagation to be negligible, one must have a thin boundary layer; that is,  $\delta_2 \ll D$ . If it is assumed that  $\delta_2 \sim O(10 \text{ m})$  [obtained for an eddy viscosity of  $\nu_0 \sim O(10^{-2} \text{ m}^2 \text{ s}^{-1})$ ], the domain should at least be limited to an area deeper than 50 m. However, a typical depth for the near-coast region may be of the order of  $O(10 \text{ m})$  [20 m in the case of Lentz et al. (2001)], and the boundary layer may reach all the way up to the surface in the domain. If this is the case, or if the bottom configuration is more complex, (3.9) and (3.10) are solved numerically.

**4. Analysis of the time-averaged secondary wave field**

I average the system of equations in (2.1)–(2.4) over a wave period, and find the governing equations and boundary conditions for the mean drift to  $O(\epsilon^2)$ . They become

$$\nu_0 \overline{W_{cc}^{(2)}} - if \overline{W^{(2)}} = F + Q, \quad (4.1)$$

$$\overline{x_{at}^{(2)}} + \overline{z_{ct}^{(2)}} = 0, \quad (4.2)$$

$$\overline{W^{(2)}} = 0, \quad c = B(a),$$

$$\overline{W_c^{(2)}} = 0, \quad \text{and} \quad c = H_0. \quad (4.3)$$

Equation (4.2) is achieved by time differentiating the incompressibility condition (2.2) to second order. The homogenous form of dynamic surface boundary condition in (4.3) is obtained by taking advantage of the surface boundary condition to first order (Weber 1998; Ng 2004). The forcing function  $F$  is given as

$$F = \nu_0 [2\overline{x_c^{(1)} W_{ac}^{(1)}} + \overline{x_{cc}^{(1)} W_a^{(1)}} - 2\overline{x_a^{(1)} W_{cc}^{(1)}} - \overline{x_{ac}^{(1)} W_c^{(1)}}] + g \overline{\zeta_{aa}^{(1)} x^{(1)}}. \quad (4.4)$$

After some algebra it is found that

$$F = F_{12} C' C'' + F_{21} C' C'' + (\overline{F}_{12} + \overline{F}_{21}) |C'|^2, \quad (4.5)$$

where

$$F_{pq} = \nu_0 \left( 2 \frac{\partial x_p}{\partial c} \frac{\partial W_q}{\partial c} + \frac{\partial^2 x_p}{\partial c^2} W_q - 2x_q \frac{\partial^2 W_p}{\partial c^2} - \frac{\partial x_q}{\partial c} \frac{\partial W_p}{\partial c} \right) + gx_p \quad (4.6)$$

and

$$\overline{F}_{pq} = \nu_0 \left( 2 \frac{\partial x_p}{\partial c} \frac{\partial^2 W_q}{\partial a \partial c} + \frac{\partial^2 x_p}{\partial c^2} \frac{\partial W_q}{\partial a} - 2 \frac{\partial x_q}{\partial a} \frac{\partial^2 W_p}{\partial c^2} - \frac{\partial^2 x_q}{\partial a \partial c} \frac{\partial W_p}{\partial c} \right). \quad (4.7)$$

The rightmost terms in (4.4) and (4.6) result from the second-order Lagrangian pressure components. The term  $Q$  in (4.1) is the mean quasi-Eulerian pressure gradient to second order,

$$Q = g \left[ \frac{\partial \overline{\zeta_E^{(2)}}}{\partial x} \right]_{x=a} = g \frac{d\overline{\zeta_E^{(2)}}(a)}{da}. \quad (4.8)$$

The form of Lagrangian pressure gradient can either be derived from a Taylor expansion of the Eulerian surface function after Longuet-Higgins [1953, his (14)], which yields  $\zeta^{(2)} = \zeta_a^{(1)} x^{(1)} + \zeta_E^{(2)}$ , or from differentiation of the second-order part of the hydrostatic pressure  $p = \rho g(H_0 + \zeta - z)$  with respect to  $c$ , which yields  $p_c^{(2)} = \rho g(\zeta_c^{(2)} - z_c^{(2)})$ . From the second-order part of the hydrostatic pressure equation  $\partial p / \partial z = J(p, z) = -\rho g$ , one also has  $p_c^{(2)} = \rho g[x_c^{(1)} \zeta_a^{(1)} - z_c^{(2)}]$ . Hence,  $\zeta_c^{(2)} = \zeta_a^{(1)} x_c^{(1)}$ .

It is convenient to divide the solution of (4.1) and (4.3) into two parts,

$$\overline{W^{(2)}} = W_{EW} + QW_e, \quad (4.9)$$

and it is required that

$$\nu_0 (W_{EW})_{cc} - if W_{EW} = F \quad \text{and} \quad \nu_0 (W_e)_{cc} - if W_e = 1. \quad (4.10)$$

Both parts satisfy the homogenous boundary conditions of (4.3). First, (4.10) is solved; then  $Q$  is determined. By integrating (4.2) from  $c = B$  to  $c = c$ , the mean vertical drift  $\overline{w}^{(2)}$  is obtained. It is given by

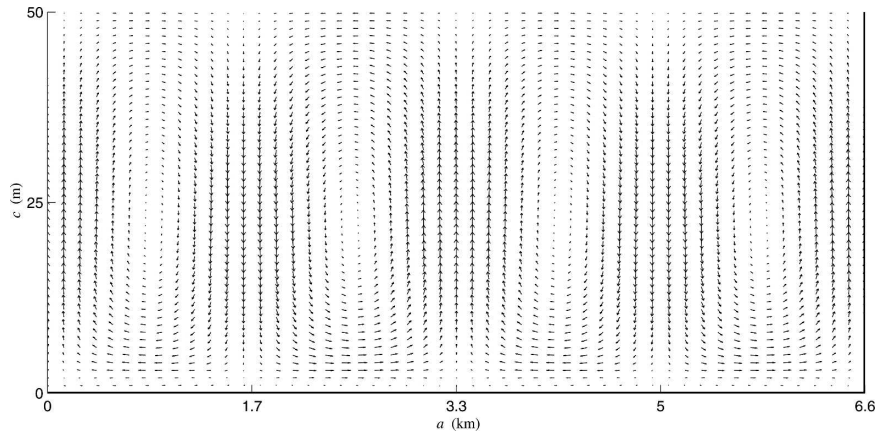


FIG. 2. The cross-shore and vertical mass transport velocity components are represented as vectors. The vertical scale is greatly exaggerated. Here, the depth is constant and equal to  $H_0 = 50$  m, the eddy viscosity is  $\nu_0 = 10^{-2} \text{ m}^2 \text{ s}^{-1}$ , and the wave period is  $T = 5$  min. The effect of rotation is ignored; i.e.,  $f = 0$ .

$$\bar{w}^{(2)} = \bar{z}_t^{(2)} = - \int_B^c \text{Re}[W_a^{(2)}] dc. \quad (4.11)$$

Thus, if the mean surface elevation is steady, the total cross-shore mass transport must be zero (e.g., Longuet-Higgins 1953; Ünlüata and Mei 1970; Weber 1998), that is,

$$\text{Re} \left[ \int_B^{H_0} \bar{W}^{(2)} dc \right] = \text{Re} \left[ \int_B^{H_0} W_{EW} + QW_e dc \right] = 0. \quad (4.12)$$

Because there can be no alongshore mass accumulation,  $Q$  must be real. Equation (4.12) then yields

$$Q = - \frac{\int_B^H W_{EW} + W_{EW}^* dc}{\int_B^H W_e + W_e^* dc}. \quad (4.13)$$

By defining  $\hat{c} = c - B$ , the wave-induced part of the solution may be written on the following form:

$$W_{EW} = \frac{e^{-mED} \sinh(m_E \hat{c})}{1 + e^{-mED} \sinh(m_ED)} j(a, D) + j(a, \hat{c}), \quad (4.14)$$

where

$$j(a, \hat{c}) = \frac{1}{\nu_0} \int_0^{\hat{c}} \int_D^{\xi} e^{m_E(2\xi - \eta - \hat{c})} F(a, \eta + B) d\eta d\xi. \quad (4.15)$$

I define  $m_E = (1 + i)/\delta_E$ , where  $\delta_E$  is the thickness of the bottom Ekman layer,  $\delta_E = (2\nu_0/f)^{1/2}$ . Then, the Ekman part of the solution may be written as

$$W_e = if^{-1} \left\{ 1 - \frac{\cosh[m_E(\hat{c} - D)]}{\cosh(m_ED)} \right\}. \quad (4.16)$$

## 5. Discussion for high-frequency shallow-water waves

I ignore the effect of rotation by letting  $f = 0$ . In this case, one has  $\omega_1 = \omega_2 = \omega$  and  $\delta_1 = \delta_2 = \delta = (2\nu_0/\omega)^{1/2}$ . The depth is taken to be constant, and terms of the order of  $\alpha/k$ , or equivalently, terms of the order of  $\delta/H_0$  are neglected. At a distance of  $L \sim \lambda = 2\pi/k$  from the coast/shore, the wave is virtually standing, and mass transport velocity to second order may approximately be written as

$$\bar{W} \cong \left( \frac{\zeta_0}{H} \right)^2 \frac{C_0}{8} \left[ -3 + 8e^{-c/\delta} \sin\left(\frac{c}{\delta}\right) + 3e^{-2c/\delta} - 9 \left( \frac{c}{2H} - 1 \right) \frac{c}{H} \right] \sin(2k\hat{a}). \quad (5.1)$$

In the notation used here, this is the uniform version of Longuet-Higgins's (1953) boundary solution [first three terms on the right-hand side of (5.1)] and his conduction solution [the parabolic terms<sup>1</sup> in (5.1)].

In Fig. 2 the mean drift field components in the  $x$ - $z$  plane, obtained from (4.9), (4.11), and (4.13)–(4.16) are

<sup>1</sup> There is a difference of a constant, resulting from the fact that Longuet-Higgins discussed the conduction (inner core) solution separately from the boundary layer solution, requiring that the net mass transport of the former to be zero.

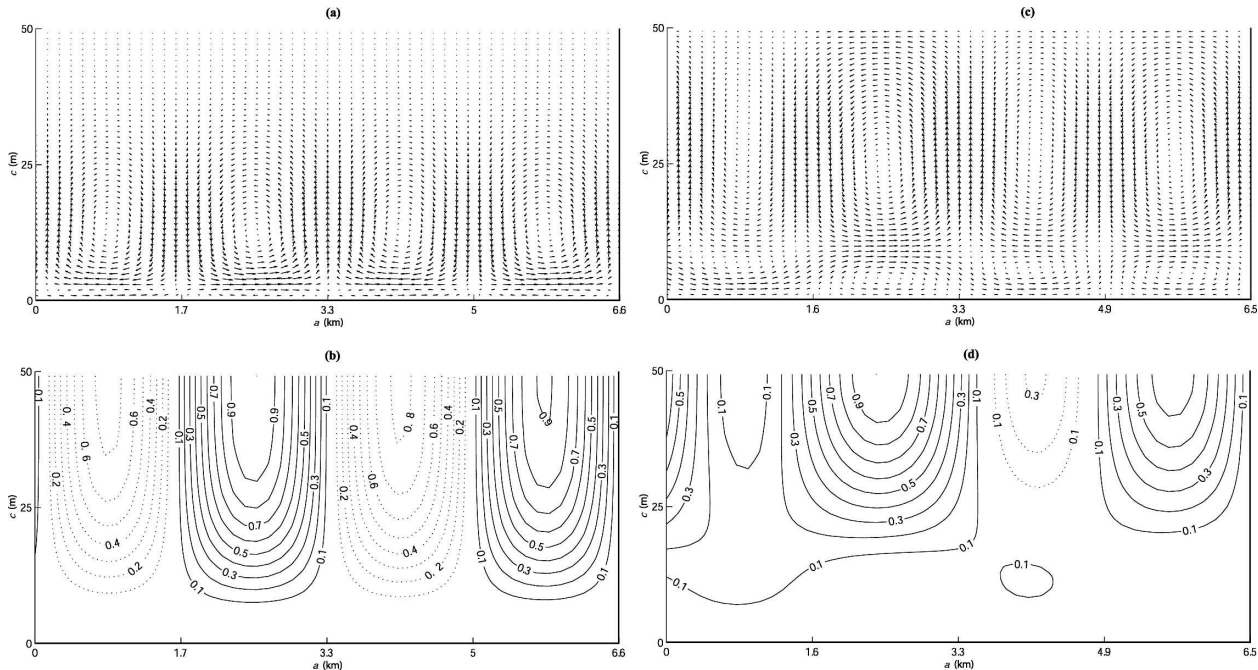


FIG. 3. As in Fig. 2, but now rotation is considered, and the alongshore component (normalized with its maximum value) is represented with a contour plot in (b) and (d). Here,  $f = 1.2 \times 10^{-4} \text{ s}^{-1}$ ; (a), (b)  $\nu_0 = 10^{-2} \text{ m}^2 \text{ s}^{-1}$ ; (c), (d)  $\nu_0 = 10^{-1} \text{ m}^2 \text{ s}^{-1}$ .

drawn as vectors. An exaggerated vertical scale is used, both for the geometry and velocity. The eddy viscosity is taken to be  $10^{-2} \text{ m}^2 \text{ s}^{-1}$ , the depth to be 50 m, and the wave period to be 5 min, and  $f = 0$ . The upper recirculation cells correspond to the cells of Longuet-Higgins's conduction solution. The lower recirculation cells, corresponding to the cells obtained from his boundary layer solution, are barely visible on this scale because of the thin wave boundary layer. The maximum magnitude of the cross-shore velocity<sup>2</sup> is here  $1.5 \text{ mm s}^{-1}$ .

Consider the same set of parameters as in Fig. 2, but now letting  $f = 1.2 \times 10^{-4} \text{ s}^{-1}$ . The results are displayed in Figs. 3a,b. This case is very similar to the nonrotating case, although the drift is geostrophically adjusted from the surface and roughly 20 m below. Here, the alongshore speed and cross-shore speed are comparable,  $\|\bar{v}\|_\infty \cong 1.4 \text{ mm s}^{-1}$  while  $\|\bar{u}\|_\infty \cong 1.2 \text{ mm s}^{-1}$ . The wave boundary layer is thin ( $\delta_2/H_0 = 0.02$ ), and the Ekman layer is significantly smaller than the depth ( $\delta_E/H_0 = 0.26$ ). The influence of friction on the Ekman part of the solution  $W_e$  must be small outside the Ekman layer. When  $H_0 \ll \delta_E$ ,  $W_e$  approximately becomes the

parabolic conduction solution of Longuet-Higgins. For  $H_0 \gg \delta_E$ ,  $W_e \cong if^{-1}(1 - e^{-mEc})$ ; see also Lamoure and Mei (1977), Weber (1998), and Hoydalsvik and Weber (2003). When one moves upward from the wave boundary layer, the boundary layer part of the solution  $W_{EW}$  must approach zero, because the forcing  $F$  approaches zero. Hence, the solution in the near-surface region is principally geostrophic and directed along the isobaths.

Increasing the eddy viscosity to  $10^{-1} \text{ m}^2 \text{ s}^{-1}$  changes the results in just the ways expected. From Figs. 3c,d we observe that the damping is stronger, and the lower recirculation cells have become more pronounced at the expense of the upper cells. Because of the increased Ekman number, the alongshore speed is reduced relative to the cross-shore speed (the maximums are 0.4 and  $1.2 \text{ mm s}^{-1}$ , respectively). The symmetry about the vertical lines under the antinodes that Longuet-Higgins (1953) obtained is notably distorted, despite the thin boundary layer ( $\delta_2/H_0 = 0.06$ ). Seemingly, when moving away from the shore, the horizontal speeds in the counterclockwise recirculation cells increase, while those in the clockwise recirculation cells decrease.

I have repeated the experiments and plotted the vector field over a few wavelengths for other depths and eddy viscosity values, and found the same feature (results not shown). Because of wave attenuation, the wave field becomes slightly more progressive as one moves away from the shore, that is, the energy of the

<sup>2</sup> As a short form of "mass transport velocity" (mean Lagrangian velocity to second order), I will use "velocity;" when referring to magnitude of this velocity, I will hereinafter use "speed."

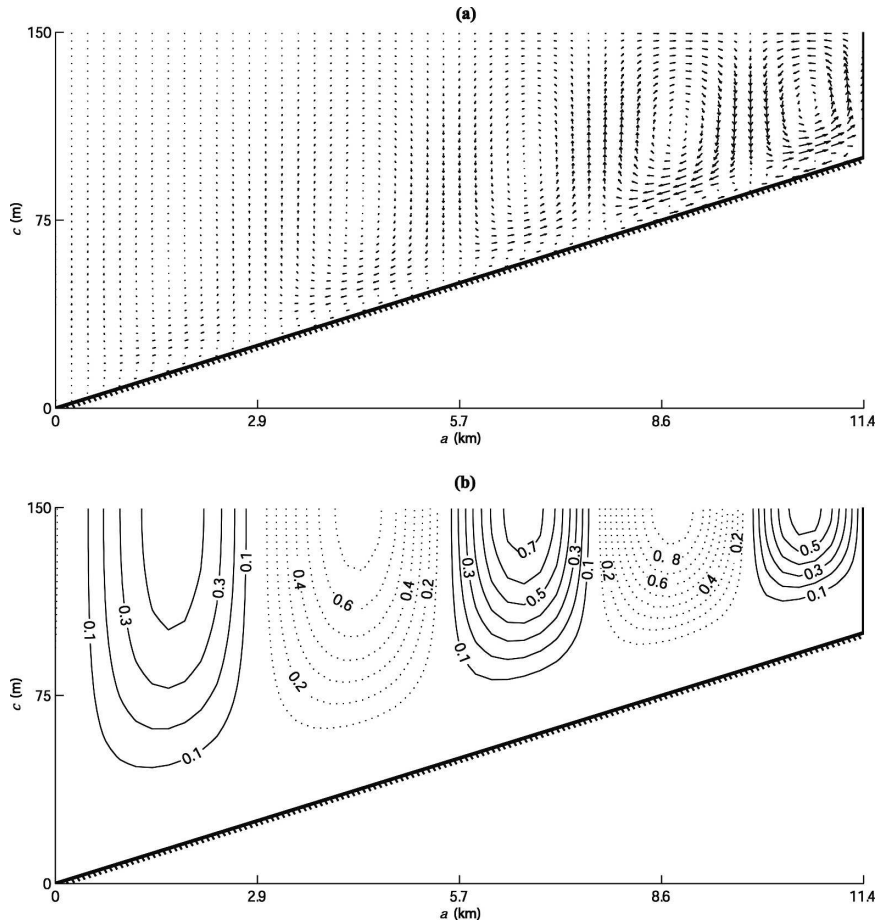


FIG. 4. As in Figs. 3c,d, but now with a linearly sloping bottom. At  $a = 0$ , the depth is  $H_0 = 150$  m. At the shore, where  $a = L = \lambda = 11.4$  km, the depth is  $H_1 = 50$  m. The bottom slope is  $\gamma = 8.7 \times 10^{-3}$ . (a) The cross-shore and vertical mean drift components. (b) The normalized alongshore mean drift component.

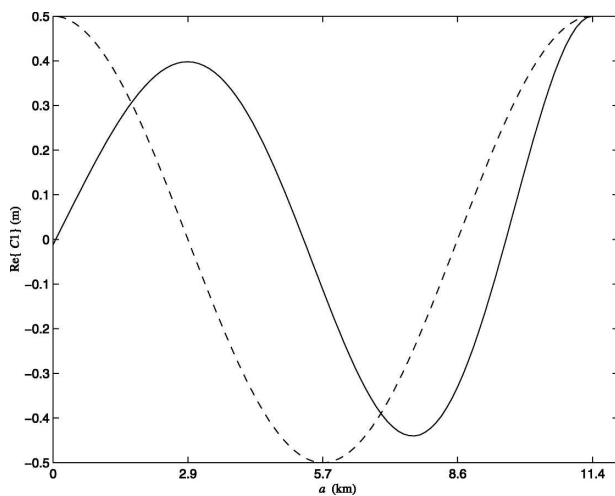


FIG. 5. The eigenfunction (4.8) obtained for the parameters used in Fig. 4 (solid line) and the trigonometric eigenfunction for constant depth  $D \equiv H_0 = 150$  m (dashed line) are plotted against  $a$ . The amplitude at the coast is 1 m.

reflected wave mode becomes smaller, while the energy of the incident mode becomes larger. Thus, the mass transport velocity profile must approach the progressive profile away from the shore (in this case directed toward the shore in the lower parts of the water body and oppositely directed in the upper parts).

I now let the bottom slope linearly from  $D = H_0 = 150$  m at  $a = 0$  to  $D = H_1 = 50$  m at  $a = L = \lambda$  (Fig. 4). Hereinafter  $\lambda = 2\pi k^{-1}$  will be used for the wavelength obtained in case of constant depth  $D \equiv H_0$ . This yields  $\gamma = 8.7 \times 10^{-3}$ . Except for the local wavenumber and the amplitude that must decrease with increasing depth, the eigenfunction (4.8) is very similar to the one obtained for a constant depth (see Fig. 5). This, of course, does not mean that the effect of topography is unimportant here; shifts in local wavenumber and energy density affect the distribution of maximum speed and the horizontal extent of the recirculation cells. (This is seen clearly from Figs. 4 and 6.)

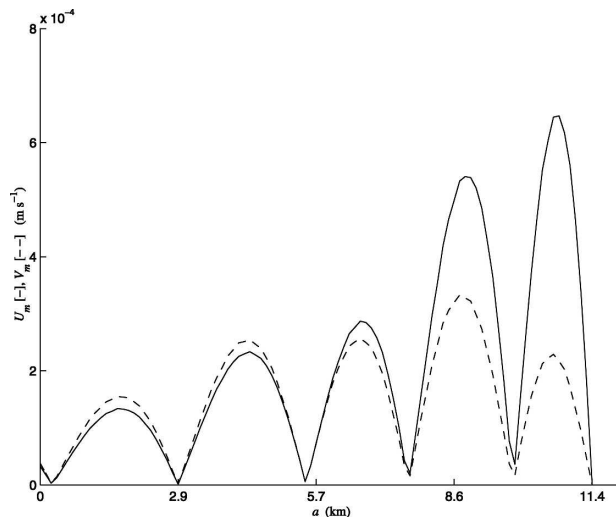


FIG. 6. Maximum mass transport velocity components over a water column,  $U_m = \|\varepsilon^2 \bar{u}^{(2)}\|_\infty$  (solid line) and  $V_m = \|\varepsilon^2 \bar{v}^{(2)}\|_\infty$  (dashed line), are plotted against  $a$  for the case of  $L = \lambda$ . The parameters are as in Figs. 4 and 5.

When  $\delta_2$  becomes comparable to  $D$  or larger, the vertical profile of the first-order solution for the velocity changes character—from hyperbolic to parabolic. This leads to a second-order solution that is different in nature. Using the trigonometric eigenfunction for waves of 5-min periods, it is found that for sufficiently small depths and large eddy viscosity values the Longuet-Higgins boundary solution goes all the way up to the surface, and the alongshore current changes direction and becomes very small in magnitude ( $\sim 1:20$  of the cross-shore magnitude). However, the depth needed for the wave boundary layer to reach the surface is far too small for us to ignore depth variations over a wavelength, even when using eddy viscosity val-

ues from the upper end of reported values. Hence, one must resort to a numerically estimated eigenfunction, taking into account both depth variation and dissipation. As an example of the combined effect of dissipation and bottom slope, I now let  $H_0 = 110$  m and  $H_1 = 10$  m. The results are displayed in Figs. 7 and 8. Many of the features seen in these figures may be expected from the results obtained for a horizontal bottom. Among others, the lower recirculation cells close to the coast reach far up into the water body, and their horizontal extension is smaller than before (Fig. 8). Relatively speaking, there are no upper cells of significance. The cell nearest to the coast goes all the way up to the surface. As anticipated from an Ekman number that is significant close to the coast (the Ekman layer is thicker than the depth), the alongshore velocity is negligible in comparison with the cross-shore velocity. The increasing energy density with decreasing depth clearly affects the overall recirculation pattern, making the two cells adjacent to the shore dominating. Moving offshore from the coast, the relative importance of the alongshore velocity in comparison with the cross-shore velocity becomes similar to that before (cf. Fig. 6 and Fig. 8).

### 6. Discussion for low-frequency shallow-water waves

I consider a hypothetical case of the  $M_2$  tidal component that is propagating on a continental shelf with constant depth and is being reflected from an infinitely long coast at right angles. Let  $D \equiv H_0 = 150$  m,  $T = 12.42$  h, and  $\nu_0 = 10^{-2} \text{ m}^2 \text{ s}^{-1}$ , and take  $L = 100$  km (Fig. 9). The cross-shore circulation is below the deepest half of the water body, and the velocity above is geostrophically balanced, as expected. Because the Ek-

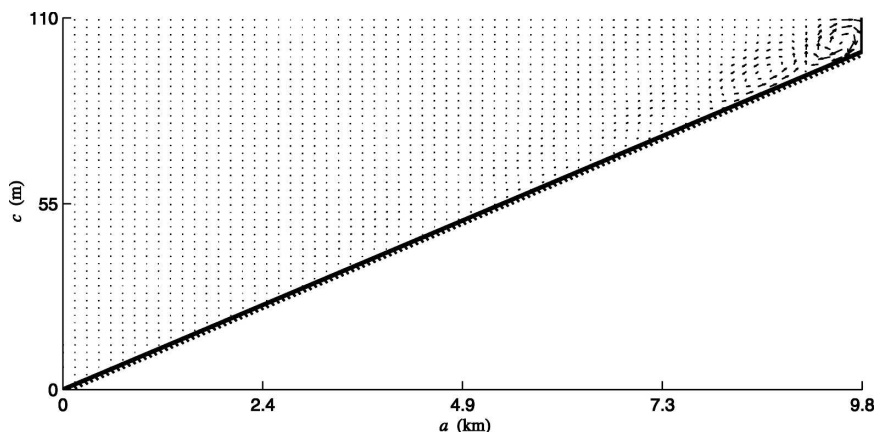


FIG. 7. As in Fig. 4a, but now  $H_0 = 110$  m and  $H_1 = 10$  m, yielding a thick boundary layer close to the coast.

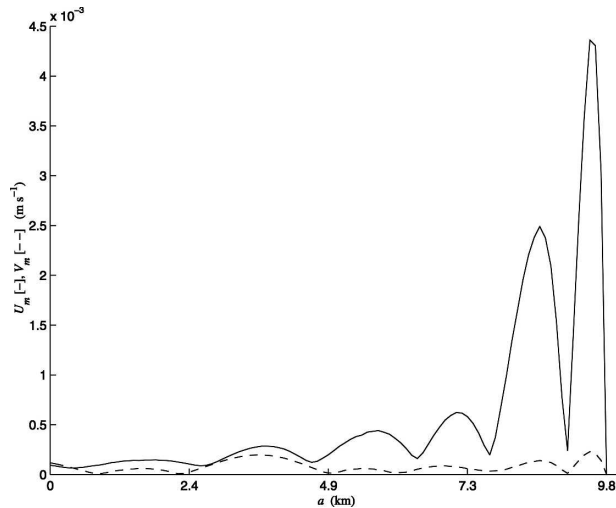


FIG. 8. As in Fig. 6, but using the same depth configuration as in Fig. 7.

man layer (about 14 m thick) is embedded in the boundary layer (about 22 m thick), one can no longer distinguish the lower and upper (semiclosed) cells (as in Fig. 3c); they have merged together, and the velocity closest to the bottom is directed *away* from the nodes, unlike the nonrotating case discussed by Longuet-Higgins (1953). The alongshore velocity here is also oppositely directed of the alongshore velocity obtained for shorter waves at shallower waters (cf. Figs. 3b and 9b).

Experiments with other frequencies have yielded the same direction of alongshore velocity for frequencies  $\omega - f \sim f$  or smaller (results not shown). Furthermore, the alongshore speed is much larger than the cross-shore speed. In the preceding example, the ratio is about 10:1. One could suspect this feature to be related to the fact that the cross-shore velocity must be zero at the coast, while  $L \ll \lambda$ ; but it is not (see Fig. 10). It is

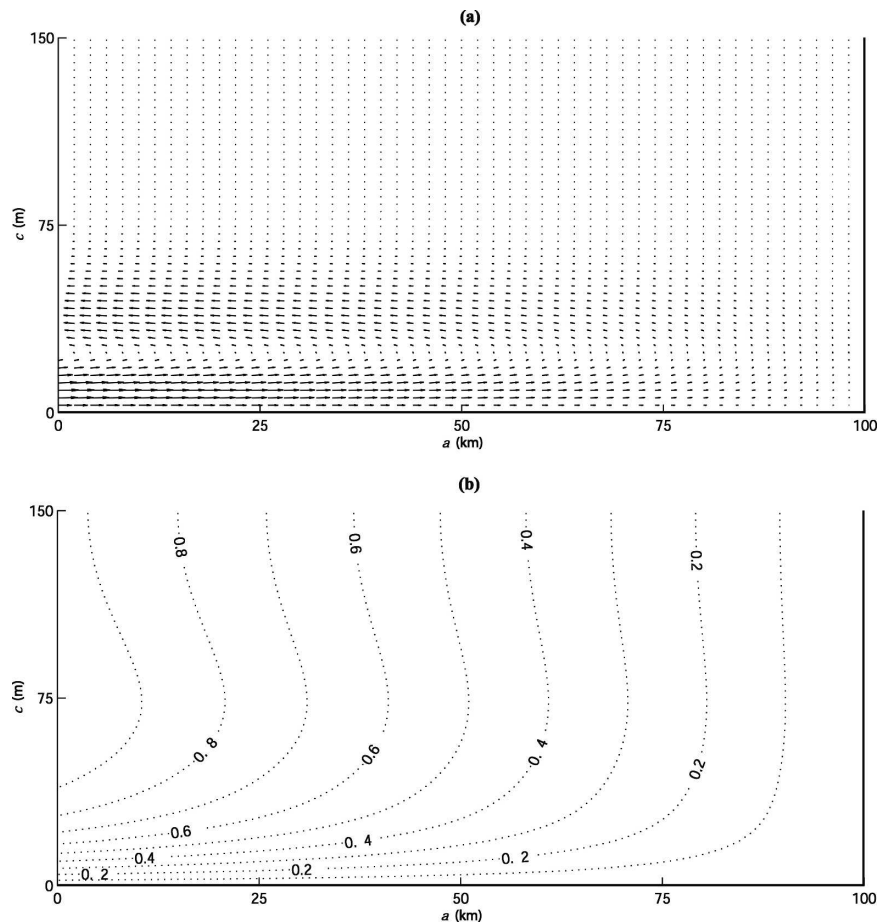


FIG. 9. The mass transport velocity for the  $M_2$  tidal component reflected from an infinite coast is considered;  $L = 100$  km. At  $a = L$ , the wave amplitude is taken to be  $A_0 = 1$  m;  $D \equiv H_0 = 150$  m,  $T = 12.42$  h,  $\nu = 10^{-2}$  m<sup>2</sup> s<sup>-1</sup>, and  $f = 1.2 \times 10^{-4}$  s<sup>-1</sup>. (a) The cross-shore and vertical mass transport velocity components. (b) The normalized alongshore mass transport velocity.

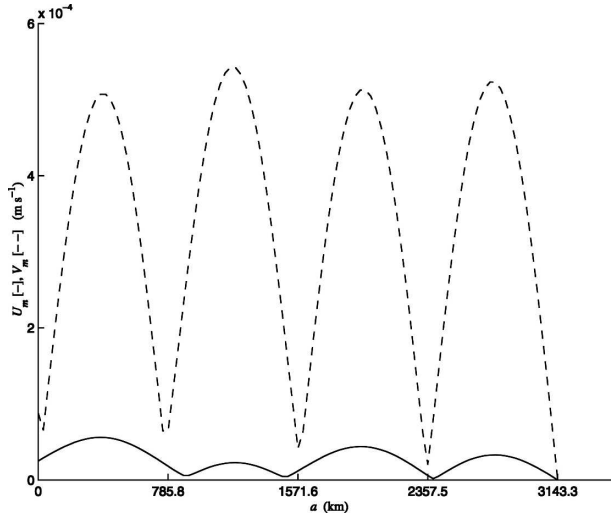


FIG. 10. The maximum magnitude of the horizontal mass transport velocity over a water column,  $U_m = \|\varepsilon^2 \bar{u}^{(2)}\|_\infty$  (solid line) and  $V_m = \|\varepsilon^2 \bar{v}^{(2)}\|_\infty$  (dashed line), is plotted against  $a$  for the case of  $L = \lambda$ . The parameters are as in Fig. 9.

concluded that the reversal of directions must be attributed to a wave frequency that is low enough for the Coriolis force to affect the primary wave field. Let us consider the mean drift in the area between the node adjacent to the coast and the antinode at the coast, that is,  $3/4\lambda < a < \lambda$ . When  $H_0 \gg \delta_E \gg \delta_2$ , the friction force dominates over the Coriolis force inside the wave boundary layer, and  $W_{EW}$  behaves like the boundary layer solution of Longuet-Higgins (1953) here. Its profile is directed toward the node just over the bottom, away from it on the top of the boundary layer, and further up until  $c \sim \delta_E$ . In the Ekman layer,  $W_{EW}$  is subject to Ekman veering<sup>3</sup> (Kundu 1976) and decays exponentially upward, because the forcing  $F$  is virtually zero outside the wave boundary layer. The net cross-shore mass transport by  $W_{EW}$  is in this case directed away from the node, along the positive  $x$  axis. Hence, the mean quasi-Eulerian pressure gradient  $-Q$  must be directed toward the node, so that the pressure-induced part of the mean flow  $W_e$  may create an Ekman transport that is directed opposite to the net cross-shore transport by  $W_{EW}$ , yielding a zero net cross-shore mass transport.

For waves with a frequency close to the inertial frequency, the Ekman layer is significantly thinner than the wave boundary layer. When  $H_0 \gg \delta_2 \gg \delta_E$ , the

<sup>3</sup> Ekman veering is the rotation of the velocity in an Ekman spiral as one moves through the Ekman layer. When moving upward, the rotation is clockwise in the bottom Ekman layer (Northern Hemisphere).

forcing  $F$  varies very slowly in the vertical, and the solution for  $W_{EW}$  can approximately be written as

$$W_{EW} \approx if^{-1}F(1 - e^{-mEc}). \quad (6.1)$$

The slow variation of forcing is related to the fact that  $\delta_2$  is its representative vertical length scale. For low frequencies and large ratios between  $\delta_2$  and  $\delta_1$ , terms with  $\delta_1$  as the typical vertical length scale become small because of large ratios between  $\omega_1$  and  $\omega_2$ . For high frequencies, the two length scales become comparable or approximately equal, so that  $\delta_2$  is still the typical vertical length scale. The forcing profile in this case is similar to that obtained for Longuet-Higgins's solution, with a strong maximum away from the node close to the bottom and an oppositely directed, weaker local maximum further up. (The profiles are not shown here.) Hence,  $W_{EW}$  is directed along the positive  $y$  axis on top of the Ekman layer, which yields a net cross-shore transport from  $W_{EW}$  that is directed toward the node because of Ekman veering. The quasi-Eulerian mean surface slope toward the shore must then be negative ( $Q < 0$ ), in order for  $W_e$  to create an oppositely directed and equally large Ekman transport. The cross-shore component for the total solution is small, because the profile of  $W_e$  roughly mirrors the profile of  $W_{EW}$  inside the Ekman layer. The geostrophically balanced solution over the boundary layer must be directed along the negative  $y$  axis.

Now the bottom is allowed to slope linearly with  $H_0 = 150$  m and  $H_1 = 50$  m, keeping the other parameter values used in Fig. 9, which yields  $\gamma = 10^{-3}$ . The mean forcing components  $F_{pq}$  in (4.5) depend only on the local water depth  $D$ , not the bottom slope  $D_a$ , and therefore have profiles that correspond to those obtained in case of a constant depth with  $H_0 = D$ . The terms marked with “ $\sim$ ” in (4.5) depend on  $D_a$ . The ratio between the latter and former terms is of the order of

$$\left| \frac{\hat{F}_{pq}}{F_{pq}} \right| \left| \frac{dC_1}{da} \right| \left| \frac{d^2C_1}{da^2} \right|^{-1} \sim \frac{D}{\delta_1}. \quad (6.2)$$

When the smallest vertical length scale associated with the primary wave field is of  $\delta_1 \sim O(10$  m), this ratio becomes of the order of 10. From this one could expect the solution to become qualitatively and quantitatively different from that obtained in the constant-depth case. However, from Fig. 11, we see that many of the qualitative features of the constant-depth case are preserved, with an alongshore current directed along the negative  $y$  axis, and a counterclockwise recirculation cell. The velocity magnitude is also preserved ( $\sim 0.1$  mm s<sup>-1</sup>). However, when the shore is approached in case of constant depth, the speed decreases linearly (it

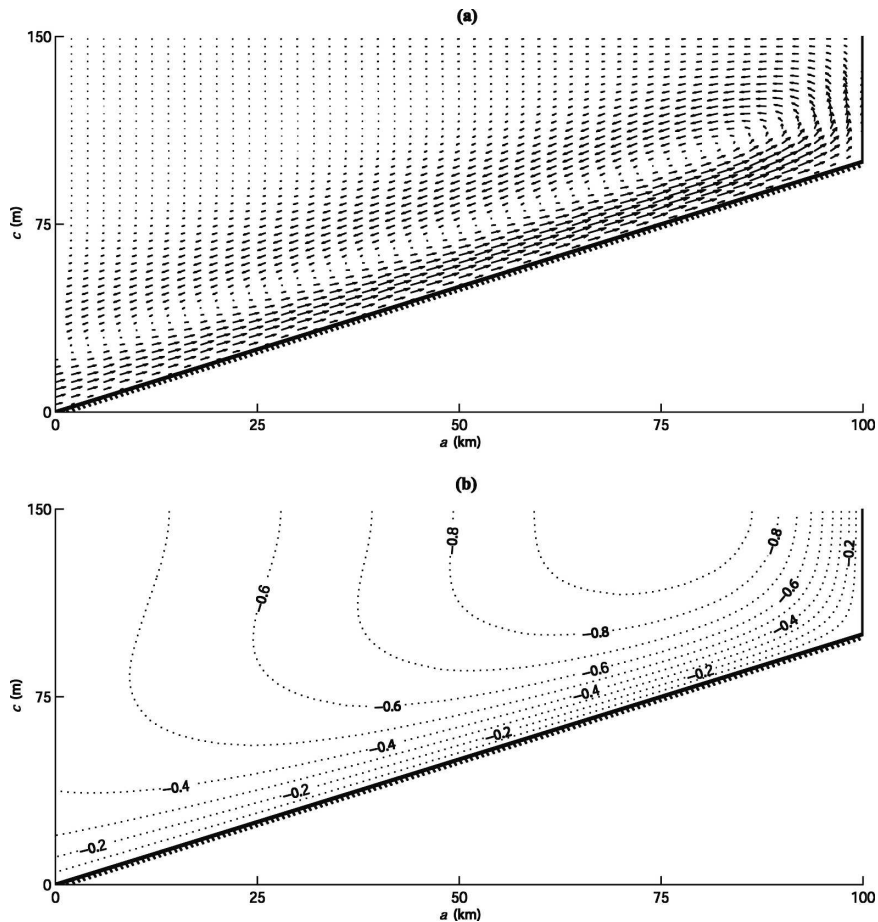


FIG. 11. As in Fig. 9, but now a linearly sloping bottom is considered. Here,  $H_0 = 150$  m and  $H_1 = 50$  m. (a) The cross-shore and vertical mass transport velocity components. (b) The normalized alongshore mass transport velocity component.

is proportional to  $\sin[2k_0(a - L)] \approx 2k_0(a - L)$  when  $\delta_2 \ll H_0$  and  $a - L \ll k_0^{-1}$ . Now the speed possesses a local maximum (its presence is evident from Fig. 11). As we recall, even in the case of waves with a period of 5 min, one did not uncover any drastic change when introducing a sloping bottom (Figs. 3 and 4). Further analysis of the forcing terms associated with a sloping bottom reveals that when the wave boundary layer is thin, the net sum of these forcing terms becomes vanishingly small. In this case, the functions in (3.7) take the following form:

$$\frac{\cosh[m_j(c - H_0)]}{\cosh(m_j D)} = \frac{e^{-m_j(c - H_0 + D)} [1 + O(e^{-2H_0/\delta_j})]}{1 + O(e^{-2H_1/\delta_j})} \approx e^{-m_j(c - H_0 + D)}. \tag{6.3}$$

For instance, if  $c \sim \delta_2 \sim H_0/10$  and  $H_1 = 2/3H_0$ , the error of the approximation for  $j = 2$  is of the order of  $\exp(-40/3) \sim 10^{-6}$ . The error of the approximation for  $j = 1$  is always equal or smaller. Then, to a vanishingly small order, one has

$$\frac{\partial W_j}{\partial a} = \frac{\partial W_j}{\partial c} \frac{dD}{da} \quad \text{and,} \tag{6.4}$$

$$\begin{aligned} \widehat{F}_{12} = v_0 \left( 2 \frac{\partial x_1}{\partial c} \frac{\partial^2 W_2}{\partial^2 c} + \frac{\partial^2 x_1}{\partial c^2} \frac{\partial W_2}{\partial c} - 2 \frac{\partial x_2}{\partial a} \frac{\partial^2 W_1}{\partial c^2} \right. \\ \left. - \frac{\partial^2 x_2}{\partial^2 c} \frac{\partial W_1}{\partial c} \right) \frac{dD}{da} = -\widehat{F}_{21}. \end{aligned} \tag{6.5}$$

The mean forcing function  $F$  consists of the same components  $F_{12}$  and  $F_{21}$  as those obtained in the constant-depth case. Because these components have the same local profile as in the case of constant depth, the mass transport velocity must also be similar to the constant-depth velocity, given that the eigenfunctions for the two cases do not behave too differently. When they do not, it may be said that the solution is of a Longuet-Higgins type, in the sense that the local mass transport profile resembles his solution (modified by rotation). Here, the eigenfunction is almost identical to that obtained in the

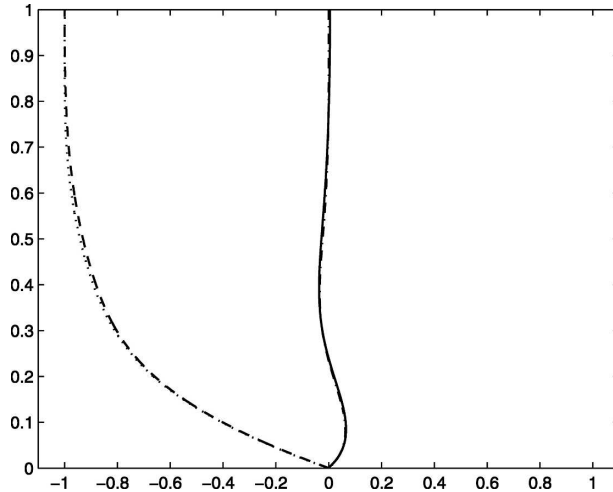


FIG. 12. The normalized profiles of the horizontal mass transport for  $a = L/2 = 50$  km, obtained using the parameters as in the former figure, are plotted together with the normalized profiles obtained for constant depth  $D \equiv H_0 = 100$  m. The vertical coordinate is  $(c - B)/D$ . Here  $a = L/2$ . Case of a sloping bottom: Cross-shore component (solid line), alongshore component (dashed line). Case of constant depth: Cross-shore component (dash-dotted line), alongshore component (dotted line).

constant-depth case, because  $L \ll k_0^{-1}, \mu^{-1}$ , and the eigenfunctions cannot vary much in the domain (results not shown). The result is almost identical mass transport profiles (Fig. 12).

From Figs. 3–5 and Figs. 9–12, and from Eq. (6.5), it is concluded that the arguments regarding the direction of the velocity induced by either gravity waves or gyroscopic-gravity waves are also relevant for the case of sloping bottom, given that the wave boundary layer is sufficiently thin (as also assumed in the discussion). The new terms in (4.5) that appear only in case of sloping bottom may be important when the wave boundary layer coincides with the whole water layer. When the boundary layer thickness becomes thinner, the sum  $\widehat{F}_{12} + \widehat{F}_{21}$  decreases exponentially. When the boundary layer thickness becomes thicker, the magnitude of the terms decreases linearly in comparison with those that appear in case of constant depth, according to (6.2).

When the bottom slope is not allowed to vary, the local wavelength that determines the horizontal extension of the recirculation pattern is either constant (for constant depth) or decreases uniformly (for linearly decreasing depth). In Figs. 9 and 11 we have seen that the recirculation induced by the tide becomes semiclosed, because its wavelength is sufficiently larger than  $L$ . However, if the bottom slope varies sufficiently, its length scale of variation can become important. As an example of this effect, a trigonometric function is now

added to the linearly sloping bottom. The results are shown in Fig. 13 (nonrotating case) and Fig. 14 (rotating case). The recirculation pattern in the nonrotating system has a flow along the bottom surface that tends to go up its slope, not unlike the recirculation pattern of Kaneko and Honji (1979) for periodic flow over a wavy wall. By comparing Figs. 13 and 14a, we see that the upper recirculation cells in deeper waters disappear when the effect of rotation is included, as is to be expected from the former discussion. The viscous recirculation cannot exist outside the wave boundary layer and the Ekman layer (see also Figs. 3a,c). Important, as we observed in the constant-depth case when the bottom Ekman layer was embedded in the wave boundary layer, the recirculation pattern is reversed relative to that obtained when  $\delta_2 \ll \delta_E$ , and the cross-shore speed is small relative to the alongshore speed. Although the model is two-dimensional, Fig. 14b suggests that the mean, along-isobath circulation around shallow areas tends to be anticyclonic, consistent with results reported earlier in literature [see Wright and Loder (1985) and references within]. The small cross-shore speed relative to the alongshore speed is also consistent with the results of Wright and Loder (1985). However, Fig. 14 also indicates that the velocity is significantly modified by shoalness and the vicinity of a steep shore.

I have also experimented with high-frequency shallow-water waves over sloping/wavy bottom with shorter bottom wavelengths, and found the same tendency—the cross-shore current immediately over the bottom, part of the lower circulation cell, tends to be directed upslope. The two-cell structure with associated alongshore velocity is similar to that found for the case of constant depth, but with the bottom crests and troughs acting as the nodes and antinodes in the constant-depth case. The magnitudes of the alongshore and cross-shore mass transport components are of the same order, just as found in the constant-depth case.

## 7. Summary and concluding remarks

Despite the idealized model setting used in this investigation, I believe that the analysis is a contribution to the understanding of mass transport velocity induced by long, barotropic ocean waves as a phenomenon. Such an understanding is important. On the one hand, the tide has a great potential ability to transport bottom sediments, because of its ubiquity and persistence. On the other hand, the modeling of the wave-induced, near-bottom mass transport in general ocean circulation models is still at an early stage.

Some of the results presented here were anticipated. For example, when one approaches the shore (i) the

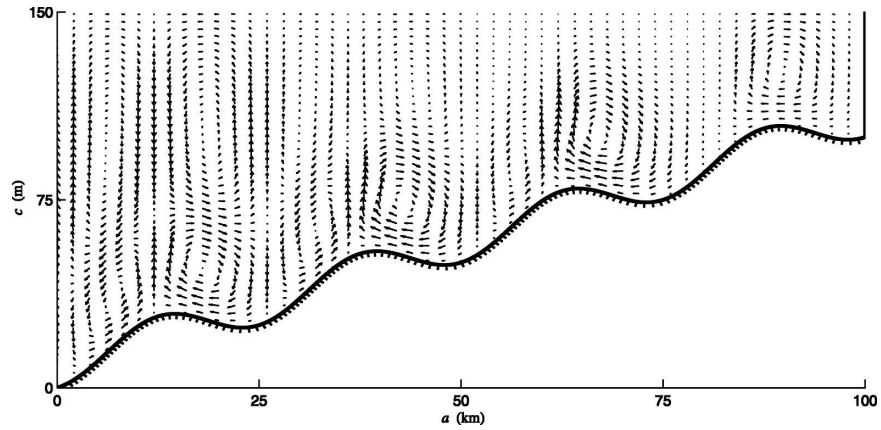


FIG. 13. As in Fig. 11, but now a trigonometric function is superimposed on the linearly sloping bottom. The bottom coordinate is  $B = \gamma a + 10 \text{ m}[1 - \cos[8\pi(a - L)/L]]$ , which yields  $D = 150 \text{ m}$  at  $a = 0$  and  $D = 50 \text{ m}$  at  $a = L$  as before. Here, the effect of the earth's rotation is excluded, i.e.,  $f = 0$ . The eigenfunction for the primary surface elevation is found numerically, taking into account the effect of dissipation.

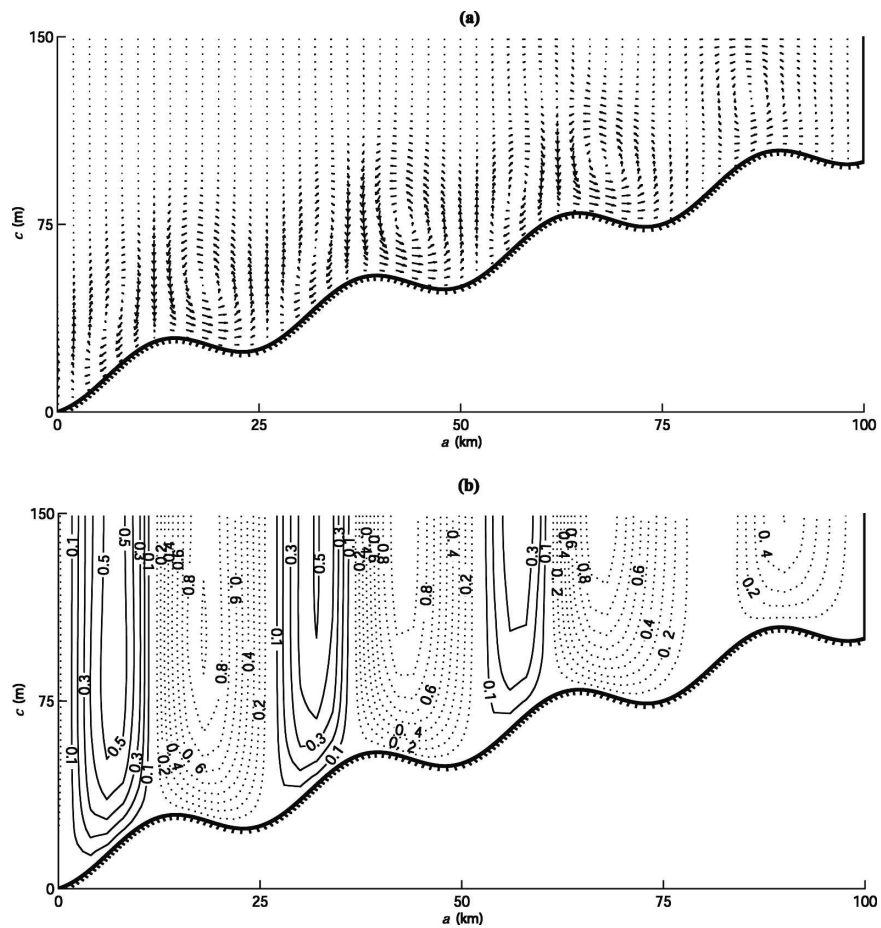


FIG. 14. As in Fig. 13, but now the effect of the earth's rotation is taken into account. Here,  $f = 1.2 \times 10^{-4} \text{ s}^{-1}$ . (a) The cross-shore and vertical mass transport velocity components. (b) The normalized alongshore mass transport velocity component.

mass transport velocity magnitude tends to increase to a maximum near the shore, (ii) the horizontal extent of the recirculation cells becomes smaller, and (iii) the Coriolis effect becomes less pronounced.

Other results are uncovered only after calculations and an in-depth analysis of the governing equations for the mass transport velocity. The mass transport velocity depends heavily on the different vertical length scales involved. For sufficiently large depths, it can be divided into two categories—that induced by frequencies comparable to the inertial frequency, and that induced by waves of much higher frequency.

In the first case, the Ekman layer is significantly thicker than the wave boundary layer. Then, the effect of the earth's rotation on the primary wave field is small. There is a lower, cross-shore recirculation cell such that the cross-shore mass transport velocity immediately over the bottom is directed toward the node (or the bottom crest in case of wavy bottom) (Figs. 3a and 13). Over this recirculation cell, there is an upper, oppositely directed recirculation cell. The alongshore mass transport velocity is directed into the paper plane when the node (or bottom crest) is to the left and antinode (or bottom trough) is to the right, and it is oppositely directed when the node (or bottom crest) is to the right and the antinode (or bottom trough) is to the left (Fig. 3b).

In the opposite case, the wave boundary layer is significantly thicker than the Ekman layer, and the effect of rotation on the primary wave field is significant. As compared with what was found for the case of a thin boundary layer, the upper recirculation cell is absent, and both the alongshore mass transport velocity and the near-bottom recirculation cell shift direction (Figs. 9 and 14). Important, it was also found that the cross-shore component of the mass transport velocity is negligible in comparison with the alongshore component (Fig. 10). For this case, the mass transport velocity is directed primarily along the isobaths.

The two main categories exist because the way momentum is transferred from the primary wave field to the mean, secondary wave field depends on the thickness of the wave boundary layer, not the thickness of the bottom Ekman layer. In contrast, the time-averaged, second-order response to this transfer depends directly on the Ekman layer thickness (and/or depth, depending on the Ekman number), and only indirectly on the thickness of the wave boundary layer, through the forcing from the primary wave field.

*Acknowledgments.* Parts of this investigation were financed by the Research Council of Norway (NFR) during the author's Ph.D. studies at the University of Oslo

(Grant 145568/432). Funding has also been provided by T. Mohn (through a private donation to the Mohn-Sverdrup Center) and, under the Aurora Mobility Program, by NFR/The French Ministry of Foreign Affairs. Drs. J. E. Weber, A. Jenkins, T. Eldevik, A. Samuelson, Ø. Sætra, M. Bentsen, J. Johannessen, and L. Bertino are acknowledged for their advices. The anonymous reviewers are greatly acknowledged for their suggestions, which not only have improved the manuscript, but also have brought this investigation forward.

## APPENDIX

### Nondimensional Formulation

Consider the cross-shore displacement  $x - a = \Delta x(a, c, t)$  and the vertical displacement  $z - a = \Delta z(a, c, t)$ . Nondimensional variables  $\hat{x} = kx$ ,  $\Delta\hat{x} = k\Delta x$ ,  $\hat{a} = ka$ ,  $\hat{y} = ky$ ,  $\hat{b} = kb$ ,  $\hat{z} = z/H_0$ ,  $\Delta\hat{z} = \Delta z/H_0$ ,  $\hat{t} = \omega t$ , and  $c = c/H_0$  are introduced. Here,  $k$  is a typical inverse length scale (e.g., wavenumber) and  $\omega$  is a typical inverse time scale (e.g., wave frequency);  $H_0$  is a typical depth. Wedged symbols without the delta in front are assumed to be of the order of 1. The cross-shore displacement must be small relative to the horizontal length scale, typically the wavelength, and the vertical displacement must be small relative to the depth, that is,  $|\Delta\hat{x}|, |\Delta\hat{z}| \ll 1$ . Let the small-amplitude surface elevation be  $\zeta = \zeta_0 \hat{\zeta}$ , where  $\zeta_0 \ll H_0$ . One has  $\hat{z} = 1 + \zeta_0/H_0 \hat{\zeta}$  at the surface, that is,  $\Delta\hat{z} = \varepsilon \hat{\zeta}$ , where  $\varepsilon = \zeta_0/H_0 \ll 1$ . The pressure term in (2.1) is of order  $-gJ(\zeta, z) \sim \varepsilon g k H_0 [1 + O(\varepsilon)]$ . If it is assumed that the acceleration term has the same order of magnitude, it is found that velocity can be written as  $W = \varepsilon \omega^{-1} g k H_0 \hat{W}$ . Casting the incompressibility condition (2.2) into nondimensional form yields

$$\begin{aligned} 1 &= x_a z_c - x_c z_a = \hat{x}_a \hat{z}_c - \hat{x}_c \hat{z}_a \\ &= 1 + \Delta\hat{x}_a + \Delta\hat{z}_c + \Delta\hat{x}_a \Delta\hat{z}_c - \Delta\hat{x}_c \Delta\hat{z}_a. \end{aligned} \quad (\text{A.1})$$

Hence,  $\Delta\hat{x}_a = -\Delta\hat{z}_c$  to leading order, that is,  $\Delta\hat{x} \sim O(\varepsilon)$ . The equation of motion (2.1) can then be written on nondimensional form as

$$\begin{aligned} \hat{W}_t + i \frac{f}{\omega} \hat{W} &= -\hat{\zeta}_a + \hat{\zeta}_a \Delta\hat{z}_c - \hat{\zeta}_c \Delta\hat{z}_a + \frac{f}{\omega} E_K \hat{W}_{cc} \\ &+ \frac{f}{\omega} E_K [2\Delta\hat{x}_a \hat{W}_{cc} + \Delta\hat{x}_{\hat{a}\hat{c}} \hat{W}_{cc} - 2\Delta\hat{x}_c \hat{W}_{\hat{a}\hat{c}} \\ &- \Delta\hat{x}_{cc} \hat{W}_{\hat{a}} + O(\varepsilon^2)] \end{aligned} \quad (\text{A.2})$$

where  $E_K$  is the Ekman number:  $E_K = \nu_0 H_0^{-2} f^{-1}$ . As stated by Pierson (1962) and Ünlüata and Mei (1970), the equation to leading order is formally equal to that obtained by neglecting nonlinear terms in the equation of motion in Eulerian coordinates. Following Pierson, one writes

$$\left. \begin{aligned} \langle \Delta \hat{x}, \Delta \hat{y}, \Delta \hat{z} \rangle &= \varepsilon \langle \hat{x}^{(1)}, \hat{y}^{(1)}, \hat{z}^{(1)} \rangle + \varepsilon^2 \langle \hat{x}^{(2)}, \hat{y}^{(2)}, \hat{z}^{(2)} \rangle + \dots \\ \hat{\zeta} &= \hat{\zeta}^{(1)} + \varepsilon \hat{\zeta}^{(2)} + \dots \\ \hat{W} &= \hat{W}^{(1)} + \varepsilon \hat{W}^{(2)} + \dots \end{aligned} \right\} \quad (\text{A.3})$$

To leading order, the solution for the velocity is oscillatory. To next order it can be divided into an oscillatory and a time-independent part. The latter part gives rise to a secular term for the displacement, a component that goes like  $\hat{x}^{(2)} \sim \hat{t}$ . Therefore, each particle cannot be followed over an unlimited amount of time. Rather, one must have  $\Delta \hat{x} = \varepsilon \hat{x}^{(1)} + \varepsilon^2 \hat{x}^{(2)} + O(\varepsilon^3)$  be small,<sup>A1</sup> that is,  $\varepsilon^2 \hat{t} \ll 1$ , or  $t \ll \varepsilon^{-2} \omega^{-1}$  (see also Longuet-Higgins 1953).

## REFERENCES

- Battisti, D. S., and A. J. Clarke, 1982: A simple method for estimating barotropic tidal currents on continental margins with specific application to the M<sub>2</sub> tide off the Atlantic and Pacific coasts of the United States. *J. Phys. Oceanogr.*, **12**, 8–16.
- Blondeaux, P., B. Maurizio, and G. Vittori, 2002: Sea waves and mass transport on a sloping beach. *Proc. Roy. Soc. London*, **458A**, 2053–2082.
- Carter, T. G., P. L.-F. Liu, and C. C. Mei, 1973: Mass transport by waves and offshore sand bedforms. *J. Waterw. Harbors Coastal Eng. Div., ASCE*, **99**, 165–184.
- Craik, A. D. D., 1982: The drift velocity of water waves. *J. Fluid Mech.*, **116**, 187–205.
- Das, P., and J. H. Middleton, 1997: Obliquely incident Poincaré waves on a sloping continental shelf. *J. Phys. Oceanogr.*, **27**, 1274–1285.
- Davies, A. M., 1985: On determining current profiles in oscillatory flows. *Appl. Math. Modell.*, **9**, 419–428.
- , S. C. M. Kwong, and J. C. Lee, 2001: A detailed comparison of a range of three-dimensional models of the M<sub>2</sub> tide in the Faeroe–Shetland channel and northern North Sea. *J. Phys. Oceanogr.*, **31**, 1747–1763.
- Dong, C., H. Ou, C. Dake, and M. Visbeck, 2004: Tidally induced cross-frontal mean circulation: Analytical study. *J. Phys. Oceanogr.*, **34**, 293–305.
- Dore, B. D., 1970: Mass transport in layered fluid systems. *J. Fluid Mech.*, **40**, 113–126.
- Grimshaw, R., 1981: Mean flows generated by a progressing water wave packet. *J. Aust. Math. Soc.*, **22B**, 318–347.
- Herbich, J. B., H. D. Murphy, and B. Van Woele, 1965: Scour of flat sand beaches due to wave action in front of sea walls. *Proc. Conf. on Coastal Engineering*, Santa Barbara, CA, ASCE, 705–727.
- Hoydalsvik, F., and J. E. Weber, 2003: Mass transport velocity in free barotropic Poincaré waves. *J. Phys. Oceanogr.*, **33**, 2000–2012.
- Hunt, J. N., and B. Johns, 1963: Currents induced by tides and gravity waves. *Tellus*, **15**, 343–351.
- Huthnance, J. M., 1973: Tidal current asymmetries over the Norfolk sandbanks. *Estuarine Coastal Mar. Sci.*, **1**, 89–99.
- , 1981: On mass transports generated by tides and long waves. *J. Fluid Mech.*, **102**, 367–387.
- Ianniello, J. P., 1979: Tidally induced residual currents in estuaries of variable breadth and depth. *J. Phys. Oceanogr.*, **9**, 962–974.
- Iskarandi, M., and L.-F. Liu, 1991: Mass transport in three-dimensional water waves. *J. Fluid Mech.*, **231**, 417–437.
- Kaneko, A., and H. Honji, 1979: Double structures of steady streaming in the oscillatory viscous flow over a wavy wall. *J. Fluid Mech.*, **93**, 727–736.
- Kundu, P. K., 1976: Ekman veering observed near the ocean bottom. *J. Phys. Oceanogr.*, **6**, 238–242.
- Lamoure, J., and C. C. Mei, 1977: Effects of horizontally two-dimensional bodies on the mass transport near the sea bottom. *J. Fluid Mech.*, **83**, 415–431.
- Lentz, S., M. Carr, and T. H. C. Herbers, 2001: Barotropic tides on the North Carolina shelf. *J. Phys. Oceanogr.*, **31**, 1843–1859.
- Liu, A.-K., and S. Davies, 1977: Viscous attenuation of mean drift in water waves. *J. Fluid Mech.*, **81**, 63–84.
- Loder, J. W., 1980: Topographic rectification of tidal currents on the sides of Georges Bank. *J. Phys. Oceanogr.*, **10**, 1399–1416.
- Longuet-Higgins, M. S., 1953: Mass transport in water waves. *Philos. Trans. Roy. Soc. London*, **A245**, 535–581.
- McWilliams, J. C., and J. M. Restrepo, 1999: The wave-driven ocean circulation. *J. Phys. Oceanogr.*, **29**, 2523–2540.
- , J. M. Restrepo, and E. M. Lane, 2004: An asymptotic theory for the interaction of waves and currents in coastal waters. *J. Fluid Mech.*, **511**, 135–178.
- Mei, C. C., 1989: *The Applied Dynamics of Ocean Surface Waves*. World Scientific, 740 pp.
- , C. Chian, and F. Ye, 1998: Transport and resuspension of fine particles in a tidal boundary layer near a small peninsula. *J. Phys. Oceanogr.*, **28**, 2313–2331.
- Ng, C.-O., 2004: Mass transport and set-ups due to partial standing surface waves in a two-layer viscous system. *J. Fluid Mech.*, **520**, 297–325.
- Pierson, W. J., 1962: Perturbation analysis of the Navier-Stokes equations in Lagrangian form with selected linear solutions. *J. Geophys. Res.*, **67**, 3151–3160.
- Pond, S., and G. L. Pickard, 1983: *Introductory Dynamical Oceanography*. Pergamon Press, 329 pp.
- Rayleigh, L., 1884: On the circulation of air observed in Kundt's tubes, and on some allied acoustical problems. *Philos. Trans. Roy. Meteor. Soc.*, **125**, 1–21.
- Restrepo, J. M., 2001: Wave-current interactions in shallow waters and shore-connected ridges. *Cont. Shelf Res.*, **21**, 1331–1360.
- Soulsby, R. L., 1983: The bottom boundary layer of shelf seas. *Physical Oceanography of the Coastal and Shelf Seas*, B. Johns, Ed., Oceanography Series, Vol. 35, Elsevier, 189–266.

<sup>A1</sup> The second term in the expression for the nondimensional horizontal displacement does not necessarily have to be small relative to its first term; the secular component of  $\hat{x}^{(2)}$  is linearly independent from the periodic terms of  $\hat{x}^{(1)}$ . However, one must always have  $|\hat{W}^{(1)}| \gg \varepsilon |\hat{W}^{(2)}|$ .

- Tee, K. T., 1985: Depth-dependent studies of tidally induced residual currents on the sides of Georges Bank. *J. Phys. Oceanogr.*, **15**, 1818–1846.
- Ünlüata, Ü., and C. C. Mei, 1970: Mass transport in water waves. *J. Geophys. Res.*, **75**, 7611–7618.
- Weber, J. E., 1998: Mass transport induced by surface waves in a viscous rotating ocean. *Free Surface Flows with Viscosity*, P. A. Tyvand, Ed., Computational Mechanics Publications, 37–67.
- Wright, D., and J. W. Loder, 1985: A depth-dependent study of the topographic rectification of tidal currents. *Geophys. Astrophys. Fluid Dyn.*, **31**, 169–220.
- Yu, J., and C. C. Mei, 2000: Formation of sand bars under surface waves. *J. Fluid Mech.*, **416**, 315–348.
- Zimmerman, J. T. F., 1978: Topographic generation of residual circulation by oscillatory (tidal) currents. *Geophys. Astrophys. Fluid Dyn.*, **11**, 35–47.
- , 1979: Euler-Lagrange transformation and the Stokes drift in the presence of oscillatory and residual currents. *Deep-Sea Res.*, **A26**, 505–520.